EXAFS, X-ray diffraction and Raman studies of $(Pb_{1-x}La_x)(Zr_{0.65}Ti_{0.35})O_3$ ($x = 0.04$ and 0.09) ceramics irradiated by high-current pulsed electron beam

V.V. Efimov[a,*], E.A. Efimova[a], K. Iakoubovskii[b], S. Khasanov[c], D.I. Kochubey[d], V.V. Kriventsov[d], A. Kuzmin[e], B.N. Mavrin[f], M. Sakharov[c], V. Sikolenko[g], A.N. Shmakov[d], S.I. Tiutiunnikov[a]

[a]*Joint Institute for Nuclear Research, 141980 Dubna, Moscow Region, Russia*
[b]*Katholieke Universiteit Leuven, Celestijnenlaan 200 D, 3001 Leuven, Belgium*
[c]*Institute of Solid State Physics, RAS Chernogolovka, Moscow Region, Russia*
[d]*Boreskov Institute of Catalysis, Lavrentiev prosp. 5, Novosibirsk, 630090, Russia*
[e]*Institute of Solid State Physics, Kengaraga str. 8, LV-1063 Riga, Latvia*
[f]*Institute of Spectroscopy, Russian Academy of Sciences Troitsk, Moscow region, Russia*
[g]*Hahn-Meitner-Institut, Glienicker str. 100, Berlin D-14109 Germany*

Abstract

We report the effect of pulsed electron beam irradiation on the long-range and short-range atomic structure, as well as on the Raman phonon modes, of perovskite $(Pb_{1-x}La_x)(Zr_{0.65}Ti_{0.35})O_3$, $x = 0.04$ and 0.09 (PLZT 4/65/35 and 9/65/35) ferroelectric ceramics. X-ray powder diffraction (XRD) spectra from the single-pulse-irradiated PLZT 9/65/35 samples reveal transformation of the cubic Pm3m ($Z = 1$) into the orthorhombic Pmmm ($Z = 1$) structure. This symmetry change is however not observed for 10-pulse irradiation performed under the same conditions: here only an increase in the coherent scattering regions, lattice volume, and the Zr–O distance distribution is observed, as revealed by XRD and X-ray absorption spectroscopy at Zr K-edge. Raman scattering from PLZT 9/65/35 ceramics is in agreement with the symmetry reduction after single-pulse irradiation and reveals significant Raman signal intensity decrease after multiple-pulse irradiation. On the contrary, no significant structural changes could be detected in PLZT 4/65/35 ceramics after single- or multiple-pulse irradiation. Possible mechanisms of pulsed electron irradiation effects in PLZT 4/65/35 and 9/65/35 ceramics are discussed.
© 2006 Published by Elsevier Ltd.

1. Introduction

Ferroelectric perovskite ABO_3 ceramics with the atomic composition $(Pb_{1-x}La_x)(Zr_{0.65}Ti_{0.35})O_3$, labeled as PLZT X/65/35, have been extensively studied because of their excellent optical, dielectric, electrooptical and piezoelectric properties [1,2]. Those properties strongly depend on the

rotations and distortions of the BO_6 octahedra [3]. Rhombohedrally distorted PLZT 4/65/35 ceramics exhibit "hard" ferroelectric behavior with the Curie temperature $T_c \sim 200\,°C$. Because of different valence of La^{3+} and Pb^{2+} ions, an enhancement in the La/Pb ratio increases the vacancy concentration and decreases the material density and phase transition temperature. Therefore, PLZT 9/65/35 ceramics ($T_c \sim 50\,°C$) is a ferroelectric relaxor characterized by a complex phase diagram, which incorporates a morphotropic phase boundary between the rhombohedral

*Corresponding author. Tel.: +7 09621 64173, fax: +7 09621 65767.
E-mail address: efimov@sunse.jinr.ru (V.V. Efimov).

and cubic phases [2]. This makes PLZT 9/65/35 ceramics extremely sensitive to external perturbations.

In this work, we precisely determine, using the powder X-ray Rietveld method, the lattice parameters and interatomic distances in PLZT 4/65/35 and 9/65/35 ceramics irradiated by high-current pulsed electron beam. In addition, the short-range order around zirconium ions is examined by extended X-ray absorption spectroscopy (EXAFS) at the Zr K-edge. The correlation between the structural changes and modifications of vibrational bands is studied by Raman spectroscopy before and after irradiation.

2. Experimental procedures

Ceramic specimens of PLZT X/65/35 (20×20 mm^2) were prepared by a two-stage hot-pressing technique from chemically coprecipitated raw materials. The samples were optically polished to 0.5 mm thickness, in order to maximize the electron irradiation effects (see a comment below), and annealed at 500 °C. The samples were stoichiometric [4] with no impurities detectable by X-ray techniques. The samples were irradiated by high-current pulsed electron beam from the Linear Inductive Accelerator LIU-3000 [5] using the following parameters: energy 800 keV, beam current 200 A, pulse duration 2×10^{-7} s, repetition rate 0.5 Hz, beam diameter 20 mm, and doses 6×10^{14} (1 pulse = 1k) and 6×10^{15} (10 pulses = 10k) electrons/cm^2 at nominal room temperature. The penetration depth of 800 keV electrons into PLZT X/65/35 ceramics is $\sim$0.5 mm [6]. Note, that the electron irradiation effects in PLZT ceramics are maximal when this penetration depth is similar to the sample thickness [7].

X-ray experimental data were collected with a Siemens D500 diffractometer (Bragg–Brentano geometry) using Cu K$_{\alpha 1}$ radiation with $\lambda = 1.5406$ Å at 30 kV, 30 mA and SiO$_2$ monochromator, Ni filter and a position-sensitive detector in steps of 0.02° at room temperature. Some X-ray diffraction (XRD) peaks were measured at Siberian Synchrotron Radiation Center using high-resolution powder diffractometer. Monochromatization of primary synchrotron radiation beam was performed by Si (1 1 1) monochromator. Radiation wavelength was 1.5398 Å. Diffractometer is equipped by Ge (1 1 1) crystal analyzer on the diffracted beam providing extremely high instrumental resolution and accuracy of data. For XRD measurements, the irradiated ceramic samples were grinded into powder. The data were analyzed using the Powder Cell program [8].

Raman spectra were measured on unirradiated and irradiated parts of the same sample using a Bruker Fourier-transform Raman spectrometer RFS100/S in a back-scattering geometry at room temperature. The spectra were excited with a 1.06 μm Nd-YAG laser operated at 200 mW.

The Zr K-edge ($E_K = 17998$ eV) EXAFS spectra were recorded at the EXAFS station of Siberian Synchrotron

Radiation Center. The storage ring VEPP-3 with electron beam energy of 2 GeV and an average stored current of 80 mA has been used as the radiation source. The X-ray energy was monochromatized with a channel-cut Si (1 1 1) crystal monochromator. The Zr K-edge EXAFS spectra were recorded in transmission mode, using two ionization chambers, filled with argon gas, as detectors. The energy step was $\sim$2.5 eV. The samples were prepared as pellets with the varied thickness to obtain a 0.7–1.0 absorption edge jump.

The EXAFS spectra were extracted using the standard procedure using the VIPER package [9]. The energy position E_0, used in the definition of the photoelectron wave number $k = (2m_e/\hbar^2[E - E_0])^{0.5}$, was set at the Zr K-edge threshold energy of 17998 eV. The Fourier transforms (FT) of the EXAFS $k^3\chi(k)$ spectra were calculated in the wave number interval $k = 2.0-12$ Å^{-1} with a Gaussian-type window function. Curve fitting procedure with IFEFFIT 1.2.6 [10] code was used to determine precisely the distance, Debye–Waller factor and coordination number in the first coordination shell of zirconium within similar wave number intervals.

3. XRD results

Fig. 1a and b shows experimental and calculated XRD profiles for the unirradiated PLZT 9/65/35 and PLZT 4/65/35 powders, respectively. The obtained structural data are given in Table 1. They are in agreement with previous studies [11].

After single irradiation of the PLZT 9/65/35 ceramics, orthorhombic [12] distortion of perovskite structure is observed (see inset of Fig. 1a), accompanied by a decrease of lattice volume and an increase of lattice strain (see Table 1). The peak broadening in irradiated 9/65/35 sample is attributed to strain and lattice distortions. It should be noted that no change in lattice symmetry, but some change growth in volume, is observed for the PLZT 9/65/35 samples after multiple irradiation (see Table 1 and Fig. 1a). Rietveld refinement of the spectrum from multiple-irradiated PLZT 9/65/35 samples revealed that both the significant decrease of the full-width at half-maximum (FWHM) and the intensity increase of all reflections are related to the value of lattice strain and size of coherent scattering regions (see Table 1), respectively. However, single and multiple irradiation of PLZT 4/65/35 ceramics do not lead to the essential structural changes (see Fig. 1b and Table 1).

4. X-ray absorption results

In the dipole approximation ($\Delta l = \pm 1$), the Zr K-edge X-ray absorption spectra are due to the electron excitations from the deep $1s$(Zr) state into the outer empty np states with $n > 4$. The EXAFS oscillations (see Fig. 2a and b), located above the edge, reflect the local atomic structure around Zr ions and are dominated by the low-frequency

signal due to the six oxygen atoms of the first coordination shell. However, the outer shells contribution is also visible in Fig. 2 as shoulders (marked by arrows) of the main oscillations, e.g., at 3.2 and 5 Å^{-1}. Single irradiation of the PLZT 9/65/35 sample (Fig. 2a) leads to a small modifica-

tion of the EXAFS oscillations, notable between 7 and 8 Å^{-1}. At the same time, multiple irradiation of the PLZT 4/65/35 sample (Fig. 2b) induces only weak modifications
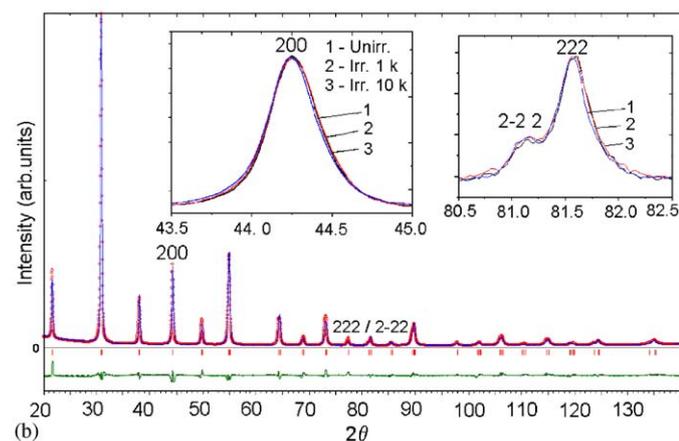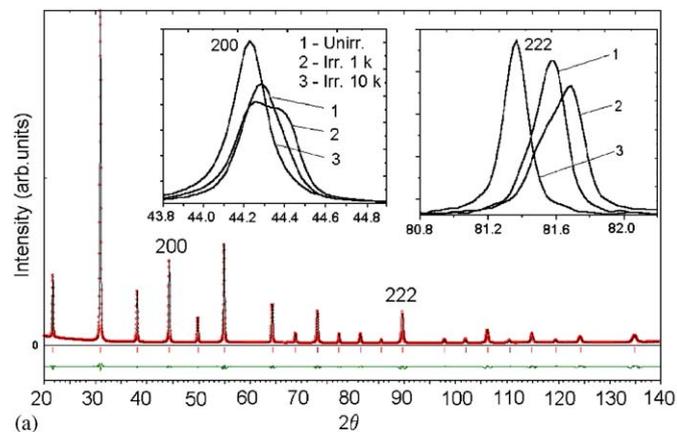

Fig. 1. Rietveld refinement plot for unirradiated PLZT 9/65/35 (a) and 4/65/35 (b). The observed and calculated patterns are shown by solid line and dots, respectively. The vertical marks show the positions of calculated reflections. The trace in bottom is a plot of the differences between the observed and calculated intensities. The insets highlight the behavior of the pseudo-cubic (2 0 0) and (2 2 2) reflections for unirradiated and irradiated by one-pulse (1k) and 10-pulse (10k) samples.
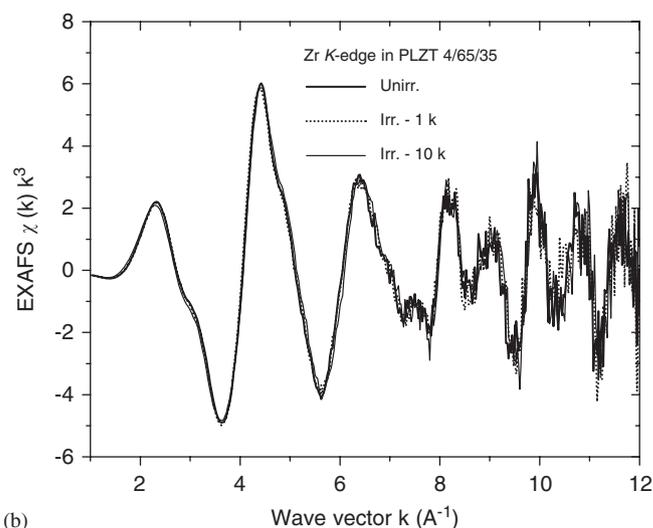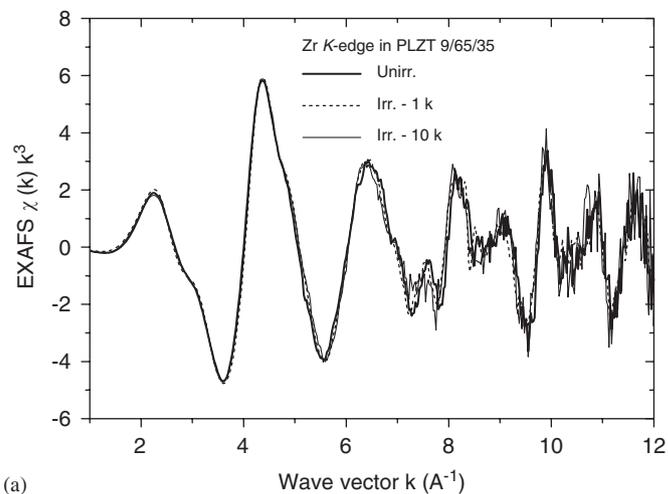

Fig. 2. Experimental EXAFS $\chi(k)k^3$ signals at the Zr K-edge in unirradiated and in single- (1k) and multiple (10k)-irradiated PLZT 9/65/35 (a) and PLZT 4/65/35 (b) powders.

Table 1
Structural parameters for unirradiated, single (1k) and multiple (10k) irradiated PLZT 9/65/35 and 4/65/35 samples

Sample	PLZT 9/65/35			PLZT 4/65/35		
Irradiation	Non-irr.	1k-irr.	10k-irr.	Non-irr.	1k-irr.	10k-irr.
Space group	Pm3m	Pmmm	Pm3m	R3m	R3m	R3m
a (Å)	4.0859 (6)	4.0912 (6)	4.0943 (6)	4.0869 (6)	4.0872 (6)	4.0871 (6)
b (Å)	4.0859 (6)	4.0826 (6)	4.0943 (6)	4.0869 (6)	4.0872 (6)	4.0871 (6)
c (Å)	4.0859 (6)	4.0726 (6)	4.0943 (6)	4.0869 (6)	4.0872 (6)	4.0871 (6)
α (deg.)	90.000	90.000	90.000	89.807	89.801	89.805
V (Å^3)	68.212	68.023	68.634	68.268	68.274	68.272
Strain, S (nm)	0.000784	0.000952	0.000373	0.00049	0.00055	0.00051
	63.4	58.2	71.4	47.7	45.3	46.1
R_{WP} (%)	7.89	8.45	7.12	8.32	9.07	9.26

S is size of coherent scattering regions, R_{WP} is a reliability factor.
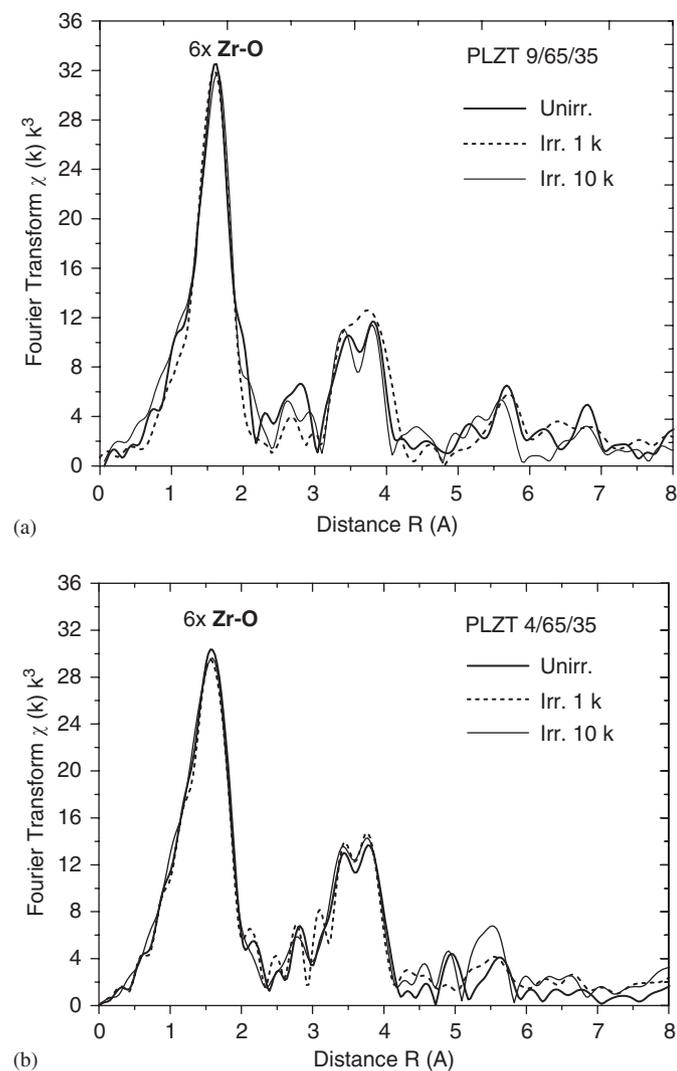
Fig. 3. Fourier transforms of the Zr K-edge EXAFS $\chi(k)k^3$ signals, shown in Fig. 2.

of the EXAFS signal, being expressed in a small increase of the oscillations frequency visible mainly at high k values.

The FT of the Zr K-edge EXAFS spectra before and after single and multiple irradiations of the PLZT 9/65/35 and PLZT 4/65/35 samples, are presented in Fig. 3a and b. They are typical for perovskite-type compounds and can be separated into three regions. The first strong peak at ~1.5 Å is due to the contribution from the first coordination shell formed by six oxygen atoms. The group of peaks in the range 2.4–4.3 Å is attributed to four contributions: (1) multiple-scattering signals generated within the first shell; (2) eight Pb/La atoms located in the second shell; (3) six Zr/Ti atoms in the third shell and multiple-scattering signals generated within Zr–O–Zr and Zr–O–Ti chains; (4) 24 oxygen atoms in the fourth shell. The peaks above 4.3 Å correspond to outer coordination shells.

The insufficient signal/noise ratio (see Fig. 2) and large number of the EXAFS signals contributing above 2.4 Å make quantitative analysis in this range rather difficult.

Therefore, we concentrated on the first-shell signal. The determined Zr–O distance is 2.05 Å and remains constant going from the unirradiated to the multiple-irradiated PLZT 9/65/35 samples (see Fig. 3). Debye–Waller factor $\sigma^2_{\text{Zr–O}} = 0.48 \times 10^{-2}$ and 0.53×10^{-2} Å^2 was found for the unirradiated and multiple-irradiated PLZT 9/65/35 sample, respectively. It should be noted, that no essential structural changes were observed for the PLZT 4/65/35 sample after multiple irradiation (see Fig. 3b).

5. Raman scattering results

Room-temperature Raman spectra before and after single and multiple irradiations of the PLZT 9/65/35 and PLZT 4/65/35 samples are shown in Fig. 4. Raman signals in cubic Pm3m perovskite structure are symmetry forbidden [13]. However, Raman scattering in disordered or glass-like systems (e.g., PLZT 9/65/35 ceramics) is allowed and is proportional to the vibration density of states [14,15], thus resulting in detectable Raman signals from PLZT 9/65/35 ceramics. The comparison of the TO1, TO2, TO3, TO4 and LO bands for unirradiated and single-irradiated PLZT 9/65/35 samples exhibits a significant increase in the peak intensity and appearance of two (see arrows in Fig. 4) additional signals, as well as a shift of the TO3 and TO4 bands to the larger wave numbers (see Fig. 4 and Table 2). These changes correlate with the Pm3m → Pmmm symmetry change detected by XRD (see Fig. 1 and Table 1). It is interesting to note that multiple irradiation of PLZT 9/65/35 leads to the abrupt decrease of integrated intensity of all Raman signals. The similar behavior of the Raman bands was observed in PLZT 8/65/35 ceramics irradiated by Nd laser with 1.02 μm and power of 10 MW [11]. It should be noted that single and multiple irradiation of PLZT 4/65/35 ceramics does not give rise to an essential Raman bands changes (Fig. 5 and Table 2).
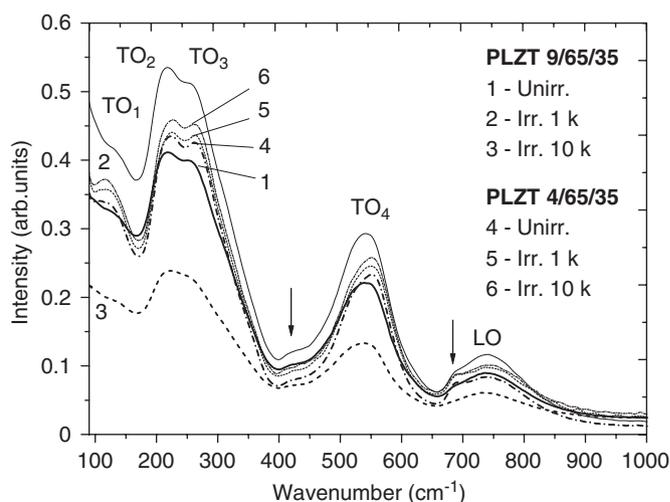

Fig. 4. Raman spectra from PLZT 9/65/35 and 4/65/35 samples before and after single (1k) and multiple (10k) irradiation.

Table 2
Raman modes (in cm^{-1}) observed in PLZT 9/65/35 and 4/65/35 samples before and after single (1k) and multiple (10k) irradiation

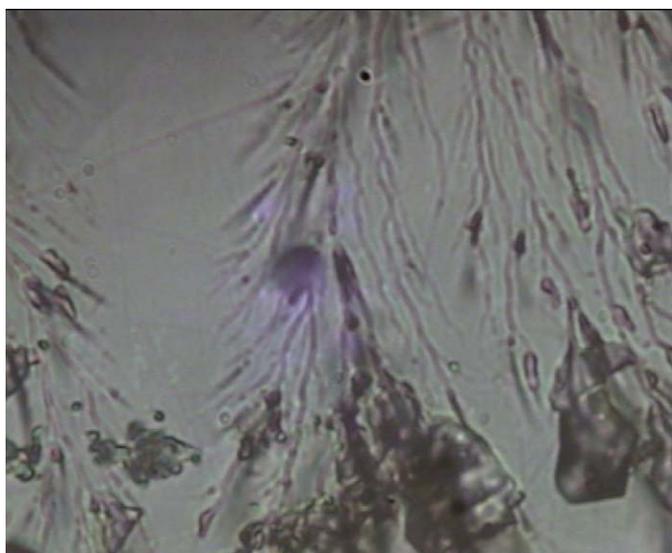| Sample	PLZT 9/65/35			PLZT 4/65/35		
Irradiation	Non-irr.	1k-irr.	10k-irr.	Non-irr.	1k-irr.	10k-irr.
TO1 Cation–Zr/TiO₃	132	132	132	116	116	116
TO2 O–Zr/Ti–O bend	215	209	215	224	210	212
TO3 O–Zr/Ti–O bend	263	258	266	263	257	264
	—	424	—	—	420	—
TO4 Zr/Ti–O stretch	556	547	555	552	548	552
		683	—	—	680	—
LO	750	750	750	750	750	750

Fig. 5. The surface of PLZT 9/65/35 ceramics after single irradiation using Laser Confocal Scanning Microscope.

6. Results and discussion

XRD, EXAFS and Raman spectroscopy results have clearly demonstrated different effect of the single and multiple irradiation on ferroelectric PLZT 9/65/35 and 4/65/35 ceramics. In this regard, it is important to note that relaxation time of secondary electrons produced in PLZT ceramics by irradiation pulse lies in the range 10^{-7}–10^{-4} s [15], i.e. it may be significantly larger than the pulse duration in our experiment (2×10^{-7} s). Therefore, we believe that single irradiation could result in accumulation of powerful spatial charge and corresponding electric fields of the order 10^{7} V/cm in the PLZT 9/65/35 samples generating dielectric breakdown and Lichtenberg figures (see Fig. 5). This electric field could also be responsible for the XRD peak splitting and corresponding symmetry lowering in the single-pulse-irradiated PLZT 9/65/35 samples (see Fig. 1). It is important to note that direct observation of such XRD peak splitting under rather moderate electric fields of $\sim$10 kV/cm has already been reported [12,16].

Another important remark regarding the single-pulse irradiation is that both the pulse duration (2×10^{-7} s) and electron–ion relaxation processes ($\sim$$10^{-11}$ s) in PLZT ceramics are much faster than the acoustic discharge processes ($\sim$$4 \times 10^{-5}$ s). Therefore, this material cannot release energy, accumulated under pulsed electron irradiation, by usual thermal expansion. Instead, due to the asymmetric shape of the vibrational potential, the sample compression or so-called thermal shock phenomenon is observed [7] with the compressive stresses estimated as $\sim$3 GPa. This model naturally explains why the lattice volume of the single-irradiated PLZT 9/65/35 sample becomes smaller in comparison with unirradiated one (see Fig. 1 and Table 1).

As to the multiple-irradiated PLZT 9/65/35 ceramics, we attribute the differences in the irradiation effects, as compared to the single-pulse electron irradiation, to the irradiation-induced annealing [7]. It has been noted that multiple irradiation can result in gradual heating of the PLZT samples up to $\sim$600 °C accompanied by significant increase in diffusion of vacancies and interstitials [17]. The latter could lead to the recrystallization and corresponding increase of lattice volume and coherent scattering regions in multiple-irradiated PLZT 9/65/35 sample (see Table 1), as compared to unirradiated and single-irradiated materials.

Finally, we would address the remarkable irradiation stability of the PLZT 4/65/35 ceramics revealed in Fig. 1 and Table 1. As discussed in the Introduction section, this enhanced stability could possibly be attributed to the "hard", rhombohedrally distorted lattice structure and significant smaller vacancy concentration.

Acknowledgments

References

[1] D.S. Corker, et al., J. Phys.: Condens. Matter 10 (1998) 6251.

[2] A. Sternberg, A. Rubulis, et al., Ferroelectrics 90 (1989) 89.

[3] M. Kunz, I. Brown, Solid State Chem. 115 (1995) 395.

[4] V. Fritsberg, A. Sternberg, L. Shebanov, A. Dobre, Ferroelectrics 34 (1981) 153.

[5] A.A. Kaminsky, V.P. Sarantsev, A.P. Sergeev, Part. Accel. 33 (1990) 189.

[6] V. Efimov, A. Sternberg, S.I. Tiutiunnikov, et al., Ferroelectrics 285 (2004) 265.

[7] V.I. Boiko, A.N. Valyev, A.D. Pogrebnyk, Sov. Phys. Usp. 42 (1999) 11.

[8] W. Kraus, G. Nolze, J. Appl. Crystallogr. 29 (1996) 301.

[9] K.V. Klementev, J. Phys. D: Appl. Phys. 34 (2001) 209–217.

[10] J. Rehr, S. Zabinsky, R. Albers, J. Am. Chem. Soc. 113 (1991) 5135.

[11] V.V. Efimov, et al., Phys. Status Solidi C 2 (2005) 449.

[12] E.T. Keve, K.L. Bye, J. Appl. Phys. 46 (1975) 810.

[13] B. Gross, Phys. Rev. B 107 (1957) 368.

[14] J.-L. Dellis, et al., J. Phys.: Condens. Matter 6 (1994) 5164.

[15] V. Dimza, G. Miller, J. Phys.: Condens. Matter 8 (1996) 2887.

[16] E.T. Keve, A.D. Annis, Ferroelectrics 5 (1973) 77.

[17] A. Sternberg, L. Shebanov, E. Birks, et al., Ferroelectrics 153 (1994) 309.